Vibronic and Vibrational Coherence and Relaxation Dynamics in the TCNE−HMB Complex

M. Hayashi,[†] T.-S. Yang,[†] J. Yu,[‡] A. Mebel,[†] R. Chang,[†] S. H. Lin,*[,†,§,⊥] Igor V. Rubtsov,[||] and K. Yoshihara[||]

Institute of Atomic and Molecular Sciences, Academia Sinica, P. O. Box 23-166, Taipei, Taiwan 106, R.O.C.; Department of Chemistry, National Kaohsiung Normal University, Kaohsiung, Taiwan, R.O.C.; Department of Chemistry, National Taiwan University, Taipei, Taiwan 106, R.O.C.; Department of Chemistry and Biochemistry, Arizona State University, Tempe, Arizona, 85287-1604; and Japan Advanced Institute of Science and Technology, Tatsunokuchi, Ishikawa 923-12, Japan

Received: November 17, 1997; In Final Form: February 4, 1998

In a previous paper, we have performed the molecular orbital calculation for the TCNE−HMB complex to find that there exist two charge-transfer (CT) states separated by only a few hundred wavenumbers, and based on this model, we have analyzed the steady-state absorption and fluorescence spectra. In this paper, we shall use this model to analyze the femtosecond fluorescence profiles reported by Rubtsov and Yoshihara and the femtosecond pump-probe time-resolved spectra reported by Wynne et al. For this purpose, vibrational relaxation, vibrational coherence, and electronic relaxation and vibronic coherence between the two CT states are considered. For the case of the TCNE−HMB complex in a nonpolar solvent, we find that the vibrational coherence is due to the 159−161.7 cm^{-1} mode, which has a vibrational relaxation time of 0.1−0.2 ps. We also find that the interaction energy between the two CT states is 50−80 cm^{-1}, which leads to internal conversion from CT2 to CT1 and back electron transfer from the CT1 to the ground electronic state with a time constant of 11.2 ps.

1. Introduction

A main feature of EDA (electron donor−acceptor) complexes is the appearance of a new absorption band due to the complex formation. Introducing the concept of charge-transfer complex, Mulliken and others reported the mechanism of the new complex formation in solution.[1−4] However, molecular orbital theory allows a more general description of such complex revealing the mechanism of complex formation.

One of the most studied EDA complexes is tetracyanoethylene−hexamethylbenzene (TCNE−HMB). Resonance Raman profiles and their analyses on this EDA complex have been reported.[5−10] The weak, near-infrared fluorescence spectrum of this system has also been measured.[6,7] Although the CT spectrum of this complex does not exhibit distinctive multiple peaks, the two closely spaced CT transitions were found on the basis of the quantum chemistry calculation.[11]

In a previous paper,[12] we have reported the results obtained from both semiempirical and ab initio calculations of the TCNE−HMB complex and discussed important features of the two CT states. From the ab initio calculation, we have identified all the vibrational modes of the electronic ground state. In particular, we have reported 23 vibrational modes in the range smaller than 310 cm^{-1}. Based on the characteristics of these modes, we divided them into three groups: (1) five donor−acceptor relative motions (DA modes) and two DA modes highly mixed with a HMB C−CH_3 twisting motion (DA/CH_3 modes); (2) 14 HMB and/or TCNE highly localized modes in the range larger than 80 cm^{-1} but smaller than the thermal energy of room temperature; (3) 2 TCNE modes smaller than 310 cm^{-1}. We should note that all DA and DA/CH_3 modes were found in the range less than 100 cm^{-1}.

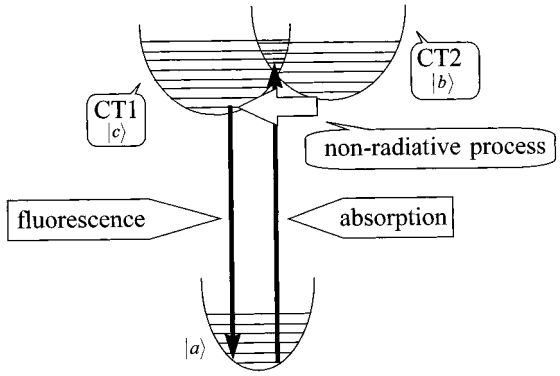

Figure 1. Model of TCNE−HMB complex in nonpolar solvent.

Based on these MO calculations, we have set up a model which is qualitatively shown in Figure 1. Using this model and the results from the resonance Raman scattering,[5−7] we have analyzed the experimental absorption and fluorescence spectra of the TCNE−HMB complex in CCl_4.

Recently, Hochstrasser's group[13] have used ultrashort pump-probe measurements to study the TCNE−HMB complex in polar and nonpolar solvents. In particular, the ultrashort time-resolved spectra of the TCNE−HMB complex in cyclohexane clearly showed quantum beats of a damped oscillation with $\hbar\omega = 161.7$ cm^{-1}. In addition to this vibrational coherence, short-time decay and long-time decay components were observed.

[†] Academia Sinica.
[‡] National Kaohsiung Normal University.
[§] National Taiwan University.
[⊥] Arizona State University.
[||] Japan Advanced Institute of Science and Technology.

S1089-5639(98)00234-5 CCC: $15.00
Published on Web 04/17/1998

More recently, Rubstov and Yoshihara[14] have reported the ultrashort time-resolved fluorescence spectra of the TCNE−HMB complex in CCl_4 solvent. They found that the time-resolved spectra showed quantum beats of 159 cm^{-1} with an ultrafast decay component.

In this paper, we shall analyze these femtosecond time-resolved spectra by using the model shown in Figure 1. From Figure 1, we can see that the ultrafast dynamics must take place between the CT1 and CT2 manifolds. In other words, in the picosecond range, we must consider the dynamics of vibrational relaxation, vibrational coherence, and vibronic coherence.

2. Ultrafast Time-Resolved Spectra

2.a. Ultrafast Pump-Probe Spectra. In the pump-probe experiments, for the case in which the pump-pulse and probe pulse do not overlap, we can use the so-called generalized linear response theory in which the time-dependent linear susceptibility includes the contributions from the dynamics of population and coherence of the system.

Using the perturbative density matrix method for the optical processes and applying the adiabatic and the Condon approximations, we obtain[15−17]

$$\vec{\vec{\chi}}''(\omega_{pu},\omega_{pr},\tau) = \vec{\vec{\chi}}''_{in}(\omega_{pu},\omega_{pr},\tau) + \vec{\vec{\chi}}''_{vco}(\omega_{pu},\omega_{pr},\tau) + \vec{\vec{\chi}}''_{eco}(\omega_{pu},\omega_{pr},\tau) \quad (1)$$

where

$$\vec{\vec{\chi}}''_{in}(\omega_{pu},\omega_{pr},\tau) = (\vec{\mu}_{ba} \otimes \vec{\mu}_{ab}/\hbar)\sum_{v} \mathrm{Re}\{\rho_{bv,bv}(\omega_{pu},\tau) \times F_{bv,bv}(\omega_{pr})\} \quad (2)$$

$$\vec{\vec{\chi}}''_{vco}(\omega_{pu},\omega_{pr},\tau) = (\vec{\mu}_{ba} \otimes \vec{\mu}_{ab}/\hbar)\sum_{v}\sum_{v' \neq v} \mathrm{Re}\{\rho_{bv,bv'}(\omega_{pu},\tau)\, F_{bv,bv'}(\omega_{pr})\} \quad (3A)$$

$$\vec{\vec{\chi}}''_{eco}(\omega_{pu},\omega_{pr},\tau) = (\vec{\mu}_{ca} \otimes \vec{\mu}_{ab}/\hbar)\sum_{v}\sum_{w} \mathrm{Re}\{\rho_{bv,cw}(\omega_{pu},\tau)\, F_{bv,cw}(\omega_{pr})\} \quad (3B)$$

Here ω_{pu} and ω_{pr} denote the central frequencies of the pump pulse and the probe pulse, respectively, τ is the time delay of probe pulse relative to pump one. In eqs 2 and 3, $\rho_{bv,bv}(\omega_{pu}, \tau)$ and $\rho_{bv,bv'}(\omega_{pu}, \tau)$ are the density matrix elements of the vibrational population of the v state and the vibrational coherence of the v and v' states, respectively, while $F_{bv,bv}(\omega_{pr})$ and $F_{bv,bv'}(\omega_{pr})$ are the band-shape functions[16,17] associated with $\rho_{bv,bv}(\omega_{pu}, \tau)$ and $\rho_{bv,bv'}(\omega_{pu}, \tau)$ of the probe optical process. In eq 3B, $\vec{\vec{\chi}}''_{eco}(\omega_{pu}, \omega_{pr}, \tau)$ denotes the contribution to the generalized susceptibility from the vibronic coherence $\rho_{bv,cw}(\omega_{pu}, \tau)$. Equation 1 indicates that the ultrafast time-resolved spectra consist of the contributions from population (i.e., $\vec{\vec{\chi}}''_{in}$ through $\rho_{bv,bv}$) and coherences (i.e., $\vec{\vec{\chi}}''_{vco}$ through $\rho_{bv,bv'}$ and $\vec{\vec{\chi}}''_{eco}$ through $\rho_{bv,cw}(\omega_{pu}, \tau)$).

2.b. Coupled Master Equations for Vibrational Relaxation and Electronic Relaxation. To obtain the dynamics of the density matrix elements given in eqs 2 and 3, we have derived coupled master equations and solved them with appropriate initial conditions associated with the optical pump process.[18−21] In the previous work,[18−21] we have presented our simulation method based on the coupled master equations for vibrational population and coherence dynamics and applied the theoretical result to analyze the quantum beat observed in the femtosecond time-resolved spectra of photosynthetic bacterial reaction centers. From Figure 1, we can see that in addition to vibrational coherence, vibronic coherence will be an important dynamics after excitation. Thus, in this paper, we shall take into account vibronic coherence.

The system Hamiltonian is given by

$$\hat{H}_0 = |a\rangle\hat{H}_a\langle a| + |b\rangle\hat{H}_b\langle b| + |c\rangle\hat{H}_c\langle c| \quad (4)$$

where

$$\hat{H}_a = \sum_{u=0}^{\infty} |u\rangle\hbar\omega^a_{vib}(u + {}^1/_2)\langle u| \quad (5A)$$

$$\hat{H}_b = \sum_{v=0}^{\infty} |v\rangle\hbar\omega^b_{vib}(v + {}^1/_2)\langle v| \quad (5B)$$

$$\hat{H}_c = \sum_{w=0}^{\infty} |w\rangle\hbar\omega^c_{vib}(w + {}^1/_2)\langle w| \quad (5C)$$

The interaction between the two CT states is given by

$$\hat{V}_J = \sum_{v=0}^{\infty}\sum_{w=0}^{\infty} |v\rangle|b\rangle J_{bc}\langle c|\langle w| + h.c. \quad (6)$$

where J_{bc} represents the electronic coupling constant between the CT1 and CT2 states. Here we have used the Condon approximation.

The Liouville equation for this system without laser fields is given by

$$\frac{\partial}{\partial t}\hat{\rho}(t) = -(i\hat{L}_0 + \hat{\Gamma} + i\hat{L}_J)\hat{\rho}(t) \quad (7)$$

where $\hat{L}_0 = [\hat{H}_0,]/\hbar$, $\hat{L}_J = [\hat{V}_J,]/\hbar$, and $\hat{\Gamma}$ represents the damping operator.[18−21] Vibrational population and coherence dynamics and vibronic coherence dynamics, as well as electronic relaxation, can be obtained by numerically solving eq 7 and by using an appropriate preparation of vibrational population and coherence and vibronic coherence created via the optical pump process.[20,21] The relevant equations of motion are given in the following, and some important relations are given in Appendixes A−C.

The coupled master equations for vibrational population, vibrational coherence and vibronic coherence are given by

$$\frac{\partial}{\partial t}\rho_{bv,bv}(t) = -\Gamma^{v,v}_{v,v}(b)\,\rho_{bv,bv}(t) - \Gamma^{v+1,v+1}_{v,v}(b)\rho_{bv+1,bv+1} - \Gamma^{v-1,v-1}_{v,v}(b)\rho_{bv-1,bv-1} - i\sum_{cw=0}^{\infty}\frac{J_{bc}}{\hbar}\langle bv|cw\rangle\rho_{cw,bv}(t) + i\sum_{cw=0}^{\infty}\frac{J_{cb}}{\hbar}\langle cw|bv\rangle\rho_{bv,cw}(t) \quad (8)$$

$$\frac{\partial}{\partial t}\rho_{bv,bv'}(t) = -\{i(v - v')\omega^b_{vib} + \Gamma^{v,v'}_{v,v'}(b)\}\rho_{bv,bv'}(t) - \Gamma^{v+1,v'+1}_{v+1,v'+1}(b)\rho_{bv+1,bv'+1} - \Gamma^{v-1,v'-1}_{v-1,v'-1}(b)\rho_{bv-1,bv'-1} - i\sum_{cw=0}^{\infty}\frac{J_{bc}}{\hbar}\langle bv|cw\rangle\rho_{cw,bv'}(t) + i\sum_{cw=0}^{\infty}\frac{J_{cb}}{\hbar}\langle cw|bv'\rangle\rho_{bv,cw}(t) \quad (9)$$

$$\frac{\partial}{\partial t}\rho_{bv,cw}(t) = -\{i(\omega_{bc} + v\omega_{\text{vib}}^{b} - w\omega_{\text{vib}}^{c}) + \Gamma_{v,w}^{v,w}(b,c)\}\rho_{bv,cw}(t) - \Gamma_{v,w}^{v+1,w+1}(b,c)\rho_{bv+1,bw+1} - \Gamma_{v,w}^{v-1,w-1}(b,c)\rho_{bv-1,bw-1} - i\sum_{cw'\neq cw}^{\infty}\frac{J_{bc}}{\hbar}\langle bv|cw'\rangle\rho_{cw',cw}(t) + i\sum_{bv'\neq bv}^{\infty}\frac{J_{bc}}{\hbar}\langle bv'|cw\rangle\rho_{bv,bv'}(t) - i\frac{J_{bc}}{\hbar}\langle bv|cw\rangle\{\rho_{cw,cw}(t) - \rho_{bv,bv}(t)\} \quad (10)$$

In this section we have presented an essential expression for transient spectra that are associated with the imaginary part of the transient susceptibility $\vec{\chi}''(\omega_{\text{pu}},\omega_{\text{pr}},\tau)$. Although we notice that multimode effects on the transient dynamics are very important due to the fact that experimentally the laser pulse widths used are in the range 80−100 fs, as a starting point we focus only on coherent excitation of one mode which has a large normal coordinate displacement. In Appendix A, taking into account other modes that have small displacements and inhomogeneities in the electronic transition frequency, we have derived an expression for the preparation of the vibrational coherence. This simplification allows us to analyze the vibrational relaxation and its characteristic time constant without involving complicated and cumbersome calculations. Our model system for the transient spectroscopy consists of three electronic states and one vibrational mode. The pump pulse interacts with the electronic ground state *a* and the CT states (Appendix A). Subsequently this optical process initiates both vibrational relaxation process in the CT2 manifold b$\{v\}$ and nonradiative transition to the CT1 manifold *c*$\{w\}$.

2.c. Ultrafast Time-Resolved Fluorescence Spectra. The signal of ultrafast time-resolved fluorescence spectroscopy which consists of the incoherent and coherent contributions can be expressed as[17,22]

$$P(\omega_{\text{scat}},t) = P_{\text{in}}(\omega_{\text{scat}},t) + P_{\text{vco}}(\omega_{\text{scat}},t) + P_{\text{eco}}(\omega_{\text{scat}},t) \quad (11)$$

where

$$P_{\text{in}}(\omega_{\text{scat}},t) = \sum_{v}\rho_{bv,bv}(t)\, f_{bv,bv}(\omega_{\text{scat}}) \quad (12)$$

$$P_{\text{vco}}(\omega_{\text{scat}},t) = \sum_{v\neq v'}\sum\rho_{bv,bv'}(t)\, f_{bv,bv'}(\omega_{\text{scat}}) \quad (13A)$$

$$P_{\text{eco}}(\omega_{\text{scat}},t) = \sum_{v}\sum_{w}\rho_{bv,cw}(t)\, f_{bv,cw}(\omega_{\text{scat}}) \quad (13B)$$

Here, $\hbar\omega_{\text{scat}}$ represents the energy of an emitted photon and the band-shape functions, $f_{bv,bv}(\omega_{\text{scat}})$, $f_{bv,bv'}(\omega_{\text{scat}})$, and $f_{bv,cw}(\omega_{\text{scat}})$ are given by

$$f_{bv,bv}(\omega_{\text{scat}}) = \frac{4\omega_{\text{scat}}^{3}}{\pi\hbar c^{3}}|\vec{e}_{\text{scat}}\cdot\vec{\mu}_{ba}|^{2}\sum_{u}|\langle bv|au\rangle|^{2}\frac{\Gamma_{b\ v,au}^{bv,au}}{(\Gamma_{b\ v,au}^{bv,au})^{2} + (\omega_{\text{scat}} - \omega_{bv,au})^{2}} \quad (14)$$

$$f_{bv,bv'}(\omega_{\text{scat}}) = \frac{2\omega_{\text{scat}}}{\pi\hbar c^{3}}|\vec{e}_{\text{scat}}\cdot\vec{\mu}_{ba}|^{2}\sum_{u}\omega_{bv',au}\omega_{bv,au}\langle bv'|au\rangle\langle au|bv\rangle[J(\omega_{\text{scat}} - \omega'_{bv',au}) + J(-\omega_{\text{scat}} - \omega'_{au,bv})] \quad (15A)$$

$$f_{bv,cw}(\omega_{\text{scat}}) = \frac{2\omega_{\text{scat}}}{\pi\hbar c^{3}}(\vec{e}_{\text{scat}}\cdot\vec{\mu}_{ca})(\vec{e}_{\text{scat}}\cdot\vec{\mu}_{ba})\sum_{u}\omega_{bv,au}\omega_{cw,au}\langle cw|au\rangle\langle au|bv\rangle[J(\omega_{\text{scat}} - \omega'_{cw,au}) + J(-\omega_{\text{scat}} - \omega'_{au,bv})] \quad (15B)$$

respectively. In eq 15, $\vec{e}_{\text{scat}}$ and $\vec{\mu}_{ba}$ represent the unit vector of the polarization of radiation and the electronic transition dipole moment, respectively, $\langle au|bv\rangle$ denotes the Franck−Condon vibrational overlap integral, and $\Gamma_{bv,au}^{bv,au}$ denotes the dephasing rate constant of the vibronic coherence between the electronically excited state bv and the ground state au. $J(\omega - \omega'_{bv,au})$ is given by

$$J(\omega - \omega'_{bv,au}) = \frac{\Gamma_{bv,au}^{bv,au}}{(\Gamma_{bv,au}^{bv,au})^{2} + (\omega - \omega_{bv,au})^{2}} + \frac{i(\omega - \omega_{bv,au})}{(\Gamma_{bv,au}^{bv,au})^{2} + (\omega - \omega_{bv,au})^{2}} \quad (16)$$

The dynamics of the population and the coherence of the system can be obtained by solving eqs 8−10.

It is instructive to derive the simplest analytic expression $P(\omega_{\text{scat}}, t)$ for a limiting case. Suppose that only $v = 1$ and $v = 0$ are coherently pumped and that we can neglect all the vibronic coupling terms in the coupled master equations. In this case, we have

$$\rho_{b0,b1}(t) = \exp(-it\omega_{10} - t\Gamma_{10}^{10})\rho_{b0,b1}(0) \quad (17)$$

$$f_{b0,b1}(\omega_{\text{scat}}) = |f_{b0,b1}(\omega_{\text{scat}})|\epsilon^{i\epsilon_{10}} \quad (18)$$

$$P_{\text{in}}(\omega_{\text{scat}},t) = \rho_{b1,b1}(t)\, f_{b1,b1}(\omega_{\text{scat}}) + \rho_{b0,b0}(t)\, f_{b0,b0}(\omega_{\text{scat}}) \quad (19)$$

$$P_{\text{vco}}(\omega_{\text{scat}},t) = 2|f_{b1,b1}(\omega_{\text{scat}})|\mathrm{e}^{-t\Gamma_{10}^{10}}\cos(t\omega_{10} + \epsilon_{10})\rho_{b0,b1}(0) \quad (20)$$

From eqs 19 and 20, we obtain

$$P(\omega_{\text{scat}},t) = A + B\mathrm{e}^{-t\gamma_{1\to0}} + C\mathrm{e}^{-t\Gamma_{10}^{10}}\cos(t\omega_{10} + \epsilon_{10}) \quad (21)$$

where $\gamma_{1\to0}$ and Γ_{10}^{10} represent the vibrational relaxation rate constant and vibrational dephasing rate constant, respectively. From eqs 15A, 16, and 18, one can see that ϵ_{10} is a function of ω_{scat} and given by $\epsilon_{10} = \tan^{-1}[\text{Im}\{f_{b0,b1'}(\omega_{\text{scat}})\}/\text{Re}\{f_{b0,b1'}(\omega_{\text{scat}})\}]$, where $f_{b0,b1'}(\omega_{\text{scat}})$ is given by eq 15A.

3. Discussions

3.a. Ultrafast Pump-Probe Spectra. Now we are in a position to analyze the femtosecond time-resolved profile of the TCNE−HMB in cyclohexane reported by Hochstrasser's group. The fs profile shows the quantum beat which has a major contribution of the damped oscillation with a frequency of $\hbar\omega = 161.7\ \text{cm}^{-1}$.[13] No obvious oscillatory components due to the coherence between $v = 0$ and $v = 2$ or the high-frequency mode coherence appears in the observed quantum beats.

Using eqs 1−3 and 8−10, we simulate femtosecond pump-probe spectra. Figure 2a shows the calculated time-resolved profile. For this simulation, we have chosen $\hbar\omega_{bc} = 400\ \text{cm}^{-1}$ from the semiempirical MO calculation[12] and $S \equiv (\omega_{\text{vib}}/2\hbar)(\Delta Q)^2 = 0.82$, Huang−Rhys factor. Here ΔQ represents a shift of the CT1 potential surface minimum with respect to the ground-state potential surface minimum along the normal

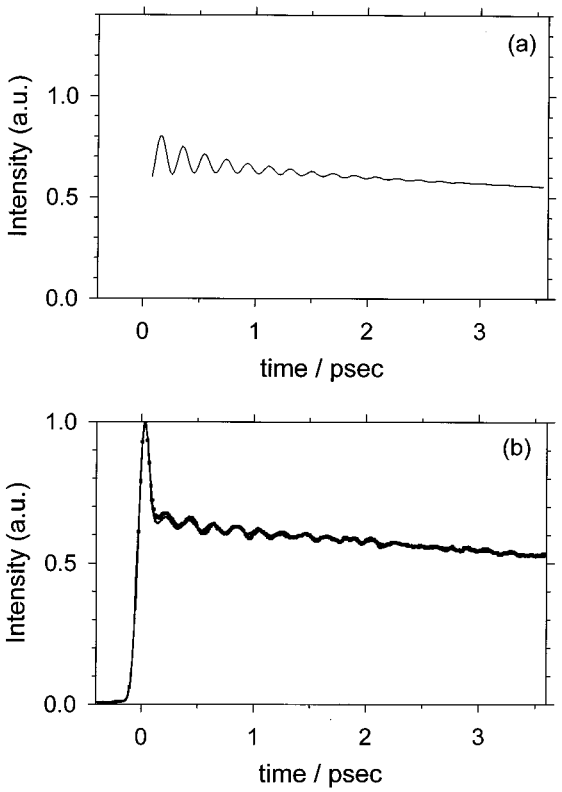

Figure 2. (a) Theoretical femtosecond time-resolved spectra and (b) experimental femtosecond time-resolved spectra.

coordinate Q of the $\hbar\omega = 161.7$ cm^{-1} mode. The value for S is determined such that no oscillatory component due to coherence $v = 0$ and $v = 2$ appears in quantum beats. The temperature is set to be 300 K. We have introduced the effective detuning $\hbar\Delta_{\text{eff}} = \hbar(\omega_{\text{pu}} - \omega_{\text{ba}})/14 = 136$ cm^{-1}, where $\hbar\omega_{\text{pu}} = \hbar\omega_{\text{pr}} = 16\,219$ cm^{-1} and $\hbar\omega_{ba} = 14\,310$ cm^{-1}, and assumed that the pump and the probe pulses have a time duration of $T_{\text{pu}} = 100$ fs with a coherence time of $1/\gamma_{\text{pu}} = 12.5$ ps^{-1} (see Appendix A). Our choice of the detuning is based on the consideration that the 161.7 cm^{-1} mode is associated with one of the 14 modes of the group (2) as mentioned in Introduction. We assume that these 14 modes can participate in the distribution of the excess energy. In Appendix A, we have derived a general expression (see eq A-5) to show the preparation of the vibrational coherence $\rho_{bv,bv'}$ by the pumping laser pulses. From this expression, we can see that the preparation of $\rho_{bv,bv'}$ depends on temperature, the Franck−Condon vibrational overlap integrals, the dispersion of inhomogeneity distribution, the dephasing constant, the laser pulse width, and the pumping frequency. In other words, these factors will determine whether a particular vibrational coherence can be prepared under the prescribed experimental conditions. That is, eq A-5 can provide the information whether a particular quantum beat under the prescribed experimental conditions can be observed.

The simulation can semiqualitatively reproduce the experimental result well if the electronic coupling constant is chosen to be $J_{cb} = J_{bc} = 2.4$ ps^{-1}, the vibrational relaxation rate constant is $\gamma_{1\to0}(\text{b}) = \gamma_{1\to0}(\text{c}) = 5$ ps^{-1}, the pure dephasing rate constant is $\gamma^{(\text{d})b} = \gamma^{(\text{d})c} = 2.5$ ps^{-1} and the vibronic pure dephasing is $\gamma_{bc}^{(d)} = 1.25$ ps^{-1}. The detailed expressions for these rate constants are given in Appendix B. Of course, we realize that the numerical values of these rate constants are valid only to within perhaps a factor of 2. But they will be helpful for further experimental investigations; for example, by varying the pumping and probing laser wavelengths in the pump−probe experiments as well as varying the pumping laser wavelength in time-resolved fluorescence experiments.

The choice of $J_{cb} = J_{bc} = 2.4$ ps^{-1} is consistent with the relative magnitudes of the transition moments of the two CT bands. We have also performed numerical calculations using values other than $J_{cb} = J_{bc} = 2.4$ ps^{-1} and found that the dynamics are insensitive to the changes of 2.4 ± 1 ps^{-1}. For comparison, the experimental results[13] are shown in Figure 2b. Our simulation can explain the behavior of the quantum beat appearing in the femtosecond profile reported by Hochstrasser's group and our simplified model grasps the essence of the experimental profile. From the displacement of the 161.7 cm^{-1} mode, a major coherence contribution comes from the coherence between $v = 0$ and $v = 1$. One cannot distinguish a contribution from impulsive stimulated Raman scattering (ISRS) from pump-probe experimental data especially when the experiment is performed under the electronically resonance condition and the vibrational dynamics of electronically excited and ground states are very similar.[23−25] In this case, inclusion of the ground-state dynamics will not seriously affect the results presented in this paper. However, our analysis on the pump-probe experiment can still be helpful for further experimental investigations such as the dependence of the pumping and probing laser wavelengths in the pump-probe experiments.

The above analysis shows that the vibrational relaxation in the two electronic states takes place at the rate of 5 ps^{-1}, while the pure dephasing rate is 2.5 ps^{-1}. The rate of vibronic transition from CT2 to CT1 is determined by the vibronic coupling J_{bc}. As seen in the above discussion, the vibrational coherence of the CT2 state is the dominant process in the short time region in our model. A significant population transition from CT2 to CT1 occurs when the coherence of CT2 is well relaxed. To see how the population of CT1 is created, we construct a long-time behavior of the vibrational population on the CT1 surface. For this purpose, one may employ a wave-packet description of the vibrational dynamics consisting of both population and coherence. The wave-packet description is easily obtained by transforming the density matrix in an energy representation to that in a normal coordinate representation, for example

$$\rho_{c,c}(Q,t) = \sum_{w=0}^{\infty}\sum_{w'=0}^{\infty} \langle Q|cw\rangle\langle cw|\rho_{c,c}(t)|cw'\rangle\langle cw'|Q\rangle$$

$$= \sum_{w=0}^{\infty}\sum_{w'=0}^{\infty} \rho_{cw,cw'}(t)\, \Psi_{cw}(Q)\, \Psi_{cw'}(Q) \qquad (22)$$

where

$$\Psi_{cw}(Q) = \left(\frac{\sqrt{\beta_c/\pi}}{2^w w!}\right)^{1/2} H_{cw}(\sqrt{\beta_c}Q)\exp(-\beta_c Q^2/2)$$

$\beta_c = \omega^c_{\text{vib}}/\hbar$, and $H_{cw}(\sqrt{\beta_c}\text{Q})$ is the Hermite polynomial. This vibrational population, $\rho_{c,c}(Q,t)$, is created via a nonradiative transition from the CT2 surface to the CT1 surface.

Figure 3 shows the simulation of time development of the vibrational population of each CT surface. Panels (a) and (b) depict the time-dependent population in a wave-packet representation and a contour map, respectively. The calculations are performed up to 10 ps. We can conclude that the nonradiative transition after 3 ps occurs from the thermally populated vibrational states of CT2, and this process does not create vibronic coherence in the CT1 surface after 3 ps. Although

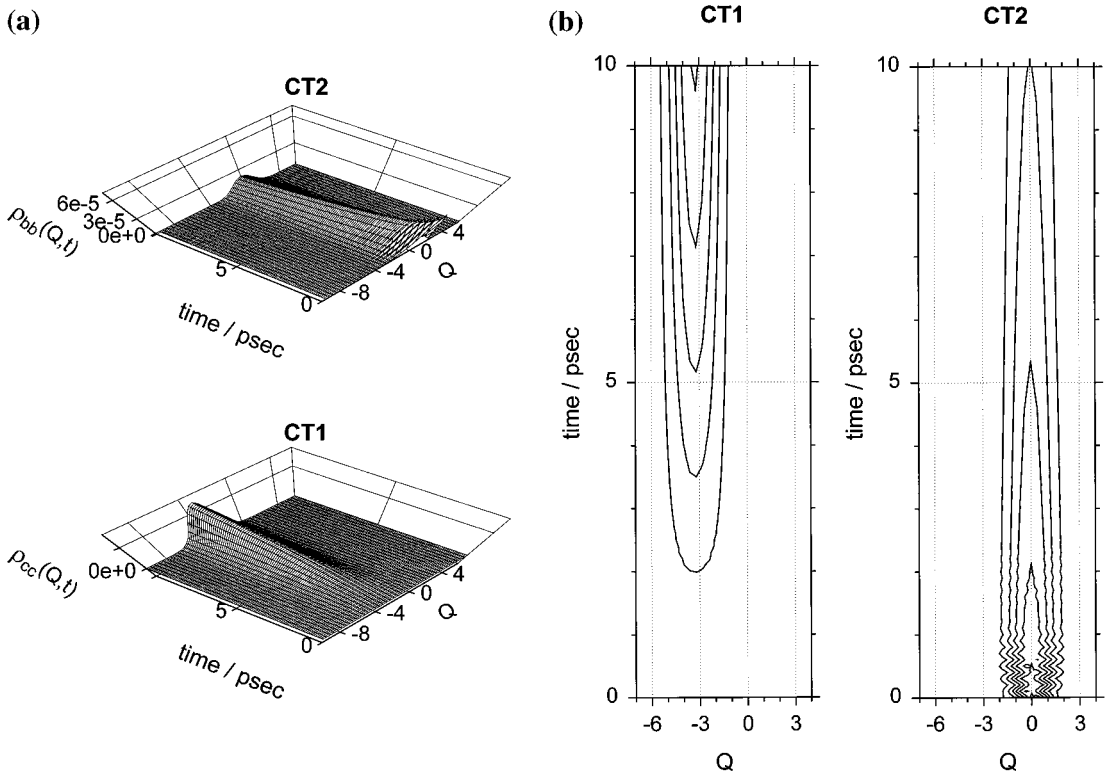

Figure 3. Long-time behavior of vibrational states of the CT1 and the CT2 surfaces. (a) A wave-packet representation of vibrational states of the CT1 and CT2 surfaces and (b) the wave-packets are shown in contour maps.

we include in our simulation a constant of 0.0892 ps^{-1} for the back-electron transfer rate constant,[13] it does not affect the CT1 dynamics at least within 10 ps. No oscillatory feature can be seen in Figure 3b after 4 ps, and then the vibrational populations increase in CT1 almost constantly. This situation indicates that the back-electron-transfer process from CT1 to the ground state occurs after the system reaches the vibrational equilibrium in CT1.

3.b. Ultrafast Time-Resolved Fluorescence Spectra. Recently, Rubtsov and Yoshihara have performed femtosecond fluorescence measurements of TCNE−HMB complex in CCl_4 and the experimentally observed femtosecond fluorescence spectra show quantum beats with an oscillation of $\hbar\omega = 159$ cm^{-1} [14] and other oscillatory components were not obviously observed. Here we shall analyze the femtosecond fluorescence spectra of the TCNE−HMB complex in CCl_4 solvent. For this purpose, we shall use the same values for the molecular variables as used in section 3.b except for dynamical quantities. The pump pulse is assumed to have a time duration of $T_{pu} = 40$ fs with a coherence time of $1/\gamma_{pu} = 25$ ps^{-1} and $\hbar\omega_{pu} = 15\,748$ cm^{-1} and $\hbar\omega_{scat} = 13\,405$ cm^{-1}. In this case, the effective detunings are -103 and 64 cm^{-1} for the excitation and the detection, respectively. The temperature is set to be 300 K.

Figure 4a demonstrates the calculated time-resolved profile. For comparison, the experimental results are reported in Figure 4b. The experimental setup and conditions are described elsewhere in detail.[14] We find that the simulation can semi-qualitatively reproduce the experimental result well with the following physical constants: $\gamma_{1\to0}(b) = \gamma_{1\to0}(c) = 6.7$ ps^{-1}, $\gamma^{(b)b} = \gamma^{(d)c} = 2.5$ ps^{-1}, $J_{cb} = J_{bc} = 1.5$ ps^{-1}, and $\gamma_{bc}^{(d)} = 1.25$ ps^{-1}. From the analysis of the transient absorption spectra of TCNE−HMB in cyclohexane and the ultrafast time-resolved fluorescence spectra of TCNE−HMB in CCl_4, we can see that certain physical constants such as electronic coupling between the two CT states and rates of vibrational relaxation show some solvent effect.

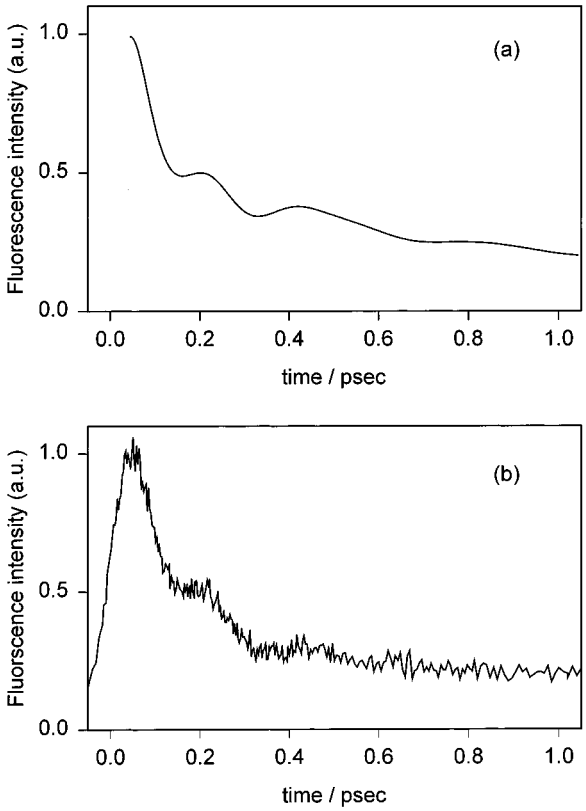

Figure 4. (a) Theoretical femtosecond fluorescence spectra and (b) experimental femtosecond fluorescence spectra.

From 4a,b, one can see a fast decay component with an oscillatory feature. To understand the detailed dynamics of this fast decay component, we also show the vibrational population

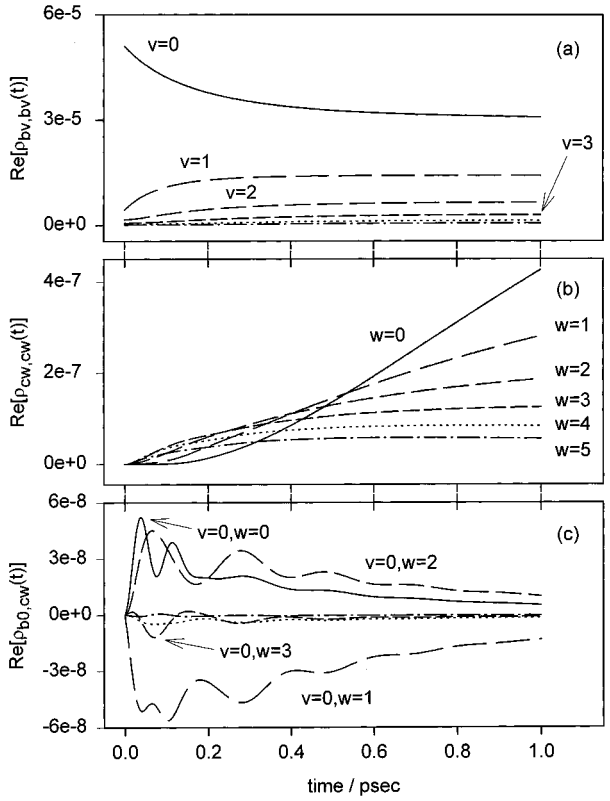

Figure 5. Vibrational and vibronic dynamics. (a) Vibrational population of CT2, (b) vibrational population of CT1, and (c) vibronic coherence of $\rho_{b0,cw}(t)$.

dynamics of both CT2 and CT1 states in Figure 5. In Figure 5, the upper panel (a) and the middle panel (b) depict the vibrational population dynamics of the CT2 state and the of the CT1 state, respectively, and the lower panel (c) shows the vibronic density matrix element $\rho_{b0,cw}(t)$ as a function of w. From Figure 5a, one can see that initially the pumping pulse creates nonequilibrated population on $v = 0$, which is larger than the pseudothermal population at 1 ps. However, other vibrational levels are less populated compared with the pseudothermal population of each level. This situation allows the $v = 0$ state to decay to the $v = 1$ state due to the thermally induced vibrational relaxation:

$$\frac{\partial}{\partial t}\rho_{b0,b0}(t) = -\mathrm{e}^{-\hbar\omega_{\mathrm{vib}}^{b}/kT}\gamma_{1\to0}(b)\rho_{b0,b0}(t) + \gamma_{1\to0}(b)\rho_{b1,b1} - i\sum_{cw=0}^{\infty}\frac{J_{bc}}{\hbar}\langle b0|cw\rangle\rho_{cw,b0}(t) + i\sum_{cw=0}^{\infty}\frac{J_{cb}}{\hbar}\langle cw|b0\rangle\rho_{b0,cw}(t) \quad (23)$$

According to our model, the ultrafast decay component in this case results mainly from the thermally induced vibrational relaxation of the $v = 0$ state.

Figure 5b shows that the vibrational populations of higher vibrational levels in the CT1 state are populated due to the vibronic coupling with the CT2 state, and subsequently, due to the vibrational relaxation, the population of $w = 0$ becomes dominant. This situation can be understood by monitoring how the vibronic coherence develops in time. From Figure 5c, we find that vibronic coherences of $v = 0 \leftrightarrow w = 0$, $v = 0 \leftrightarrow w = 1$, and $v = 0 \leftrightarrow w = 2$ play an important role in the vibronic transition from the b state to the c state.

It should also be instructive to simulate detection frequency dependence of fs fluorescence spectra based on our model. Figure 6 shows the simulated fs fluorescence spectra with

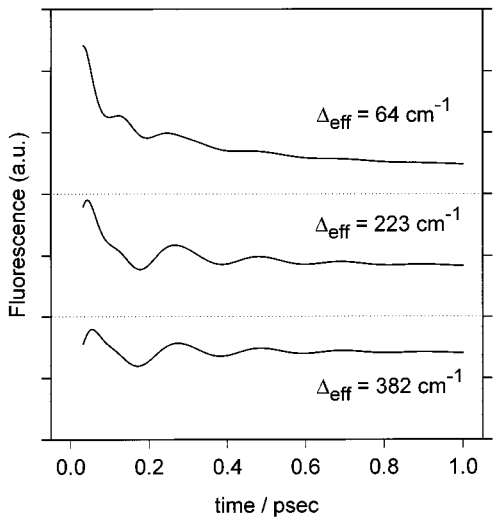

Figure 6. Detection frequency dependence of calculated femtosecond fluorescence spectra.

effective detection detuning $\hbar\Delta_{\mathrm{eff}} = 64$, 223, and 382 cm^{-1}. As discussed in the previous section, we can see phase shifts in the time-resolved spectra as a function of $\hbar\Delta_{\mathrm{eff}}$. It should be noted that the fast decay component becomes less obvious in the case in which $\hbar\Delta_{\mathrm{eff}}$ is large.

The dynamics of anisotropy for intramolecular electronic excitation-transfer processes of molecules in solution has been studied by Hochstrasser's group.[26−28] It was shown that the time-dependent fluorescence anisotropy measurement technique is a powerful tool for studying the transient excitation transfer dynamics occurring between two chromophores on a time scale of several hundreds femtoseconds.

We are now interested in the polarization effect on time-resolved fluorescence spectra of TCNE−HMB complex since the two charge-transfer states (i.e., CT1 and CT2) are closely located in energy. For this purpose, we need the following two relations which relate the space-fixed coordinates to be molecule-fixed coordinates in order to carry out the spatial averages over the molecular orientation:

$$\langle A_Z B_Z C_Z D_Z\rangle = {}^1/_{15}\,[(\vec{A}\cdot\vec{B})(\vec{C}\cdot\vec{D}) + (\vec{A}\cdot\vec{C})(\vec{B}\cdot\vec{D}) + (\vec{A}\cdot\vec{D})(\vec{B}\cdot\vec{C})] \quad (24)$$

$$\langle A_X B_X C_Z D_Z\rangle = {}^2/_{15}\,(\vec{A}\cdot\vec{B})(\vec{C}\cdot\vec{D}) - {}^1/_{30}\,[(\vec{A}\cdot\vec{C})(\vec{B}\cdot\vec{D}) + (\vec{A}\cdot\vec{D})(\vec{B}\cdot\vec{C})] \quad (25)$$

where, for example, $\vec{A}$ represents a transition dipole moment of the molecule.

We first consider a case in which both pumping and fluorescence involve the same two electronic states a and b. In this case, if both pumping and observation involve the Z-polarization, then $P(\omega_{\mathrm{scat}}, t)$ will be proportional to ${}^1/_5|\vec{\mu}_{ba}|^4$ and if the pumping is polarized along the Z-axis while the observation is polarized along the X-axis, then $P(\omega_{\mathrm{scat}}, t)$ will be proportional to ${}^1/_{15}|\vec{\mu}_{ba}|^4$. Thus, the anisotropy of this single excited state case is 0.4.

We now discuss the case of TCNE−HMB complex in which the two CT states are involved in the optical process. To see the essence of the effect of the two electronic transitions on anisotropy, we focus on the population dynamics, assuming that the system reaches the vibrational equilibrium and that only the b state is optically excited initially. In this case, the

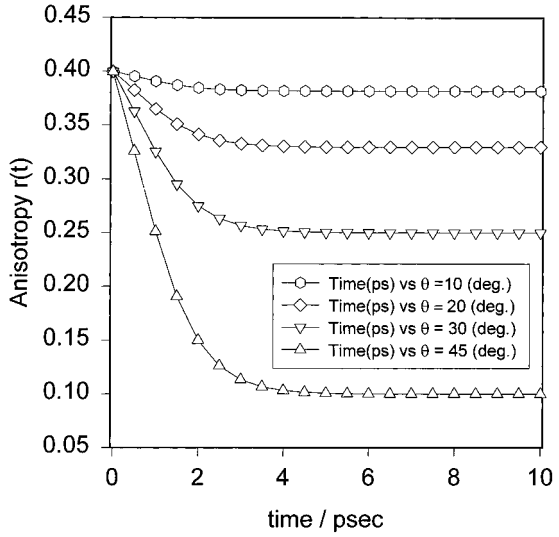

Figure 7. Calculated anisotropy of time-resolved fluorescence spectra.

dynamics of each electronically excited state is given by

$$d\rho_{bb}/dt = -W_{b\to c}\rho_{bb} + W_{b\to c}e^{-E_{bc}/kT}\rho_{cc} \qquad (26a)$$

$$d\rho_{cc}/dt = -(W_{c\to a} + W_{b\to c}e^{-E_{bc}/kT})\rho_{cc} + W_{b\to c}\rho_{bb} \qquad (26b)$$

where

$$W_{b\to c} = |J_{bc}/\hbar|^2 \int_{-\infty}^{\infty} d\tau \exp(i\tau\omega_{cb}) \prod_{l=1}^{N} G_l(t) \qquad (26c)$$

(see Appendix A, eq A-6).

If both pumping and observation involve the *Z*-polarization, then eq 24 becomes $^1/_5|\vec{\mu}_{ba}|^4$ for fluorescence from the *b* state and $((2\cos^2\theta + 1)/15)|\vec{\mu}_{ba}|^2|\vec{\mu}_{ca}|^2$ for that from the *c* state. Here, we have used $\vec{\mu}_{ba}\cdot\vec{\mu}_{ca} = |\vec{\mu}_{ba}||\vec{\mu}_{ca}|\cos\theta$. If the pumping is polarized along the *Z*-axis while the observation is polarized along the *X*-axis, from eq 25 we find $^1/_{15}|\vec{\mu}_{ba}|^4$ for fluorescence from the *b* state and $((2 - \cos^2\theta)/15)|\vec{\mu}_{ba}|^2|\vec{\mu}_{ca}|^2$ for that from the *c* state. Thus, the anisotropy will approximately be given by

$$r(t) \approx 0.4 + {}^3/_5(\cos^2\theta - 1)\frac{|\vec{\mu}_{ca}/\vec{\mu}_{ba}|^2\rho_{cc}(t)}{\rho_{bb}(t) + |\vec{\mu}_{ca}/\vec{\mu}_{ba}|^2\rho_{cc}(t)} \qquad (27)$$

Now we shall demonstrate eq 27 as a function of θ by solving eq 26. Figure 7 shows the calculated anisotropy of this system. The calculations are based on $J_{cb} = J_{bc} = 1.5$ ps^{-1} and the values for the other parameters taken from ref 12. We can see from Figure 7 that it is important to measure the anisotropy of TCNE−HMB complex in order to discuss the orientation of the transition dipole moments of the two CT states. It would also be interesting to investigate solvent effects on the anisotropy of TCNE−HMB. In this treatment, we have restricted ourselves only to the population dynamics after the thermal equilibrium is reached. However, a more sophisticated simulation including vibronic and vibrational coherences can be carried out as well.

4. Conclusion

We have shown in the previous sections that the back electron transfer from CT1 to the ground state becomes dominant when the vibrational population in CT1 reaches thermal equilibrium (or at least pseudoequilibrium) due to the fact that vibrational relaxation occurs faster than the characteristic time of electron transfer. It is more appropriate to regard this back-electron-transfer process as internal conversion because this nonradiative process goes from an excited electronic state (in this case CT1) to the ground electronic state.

We have found that the ultrafast decay component observed by Robtsov and Yoshihara is mainly due to the thermally induced vibrational relaxation from $v = 0$ to $v = 1$ in the excited electronic manifold. Detection frequency dependence and polarization dependence of femtosecond time-resolved fluorescence have also been simulated based on our model.

Note that experimental data in a much shorter time region are needed for a quantitative analysis of the amplitude and phase of the beat modulation. Such a detailed analysis will lead to a better understanding of the potential surfaces of the ground, CT1, and CT2 of TCNE−HMB. Thus, femtosecond time-resolved spectra of TCNE−HMB complex at various pump and probe frequencies are required for us to perform a more detailed analysis and to have a more critical test on the theoretical model.

From the theoretical analysis of the experimental data of the femtosecond pump-probe time-resolved spectra of a TCNE−HMB complex in cyclohexane and the femtosecond time-resolved fluorescence spectra of TCNE−HMB complex in CCl_4, we can see that the vibrational mode of 159−161.7 cm^{-1} is responsible for vibrational relaxation and dephasing and that the physical constants such as the rates of vibrational relaxation and dephasing and the electronic interaction between CT1 and CT2 are sensitive to solvents (i.e., the solvent effect).

It should be noted that the TCNE−HMB complex is an ideal system for studying the photophysical processes for the reason that absorption spectra, fluorescence spectra, resonance Raman spectra, and charge-recombination rate constant between the ground and charge-transfer states are available. The fact that the TCNE−HMB complex can be easily crystallized and that it possesses no inversion symmetry but has large dipole-moment differences between the ground and excited states (in this case CT states) may make this complex an ideal system for producing large second-harmonic generation.

Acknowledgment. This work was supported by the National Science Council of the Republic of China. We would like to thank the referee for useful comments and suggestions.

Appendix A

In this Appendix, we shall derive an expression for the preparation of vibrational coherence by the pumping lasers under an inhomogeneous condition in which there exist the electronic transition energies distributed with a Gaussian distribution function. This vibrational coherence can then be used as the initial condition in the solution of eq 9. We start with the stochastic Liouville equation which takes into account the interaction between the molecules and the laser. We assume that the pulse has a rectangular shape of its duration time T_{pu}, its coherence time $1/\gamma_{pr}$, its central frequency ω_{pu}, and its amplitude $|\vec{E}(\omega_{pu})|$.

In the following, our derivation assumes $0 \le t \le T_{pu}$. In the rotating wave approximation, we find for the off-diagonal density matrix of the vibronic coherence due to the interaction

with the laser:

$$\sigma_{bv,au}(\omega_{pu},t) = \frac{i}{\hbar}\vec{\mu}_{bv,au}\cdot\vec{E}(\omega_{pu})\rho_{au,au}(0)\frac{(1-e^{-tD_{bv,au}})}{D_{bv,au}} = \frac{i}{\hbar}\vec{\mu}_{bv,au}\cdot\vec{E}(\omega_{pu})\rho_{au,au}(0)\int_0^\infty d\tau\,\{e^{-tD_{bv,au}} - e^{-(t+\tau)D_{bv,au}}\} \quad (A\text{-}1)$$

where $\rho_{bv,au}(t) = \sigma_{bv,au}(\omega_{pu}, t)e^{-it\omega_{pu}}$, $D_{bv,au} = i(\omega_{bv,au} - \omega_{pu}) + \Gamma^{bv,au}_{bv,au} + \gamma_{pu}$, and $\Gamma^{bv,au}_{bv,au}$ represents the dephasing rate constant for the vibronic coherence between the electronically excited state bv and the ground state au.

For the Gaussian distribution of inhomogeneities, we find

$$\langle e^{-itD_{bv,au}}\rangle = \exp\left[-it(\bar{\omega}_{bv,au} - \omega_{pu}) - t\Gamma^{bv,au}_{bv,au} - t\gamma_{pu} - \frac{d^2t^2}{4}\right] \quad (A\text{-}2)$$

where $\langle\cdots\rangle$ represents the average operation, $\bar{\omega}_{bv,au} = \bar{\omega}_{ba} + (u - v)\omega_{vib}$ with $\bar{\omega}_{ba}$ being the average of the electronic transition frequency and d denotes its dispersion of Gaussian distribution for inhomogeneities.

The preparation for the vibrational coherence via the pumping laser is then given by

$$\langle\rho_{bv,bv'}(t)\rangle = \frac{i}{\hbar}e^{-tD_{bv}},_{bv'}\int_0^t d\tau\, e^{\tau D_{bv,bv'}}\sum_u [[\vec{\mu}_{bv,au}\cdot\vec{E}(\omega_{pu})]\times \langle\{\sigma_{bv'au}(\omega_{pu},\tau)\}^*\rangle - [\vec{\mu}_{au,bv'}\cdot\vec{E}(\omega_{pu})]\langle\sigma_{bv,au}(\omega_{pu},\tau)\rangle] \quad (A\text{-}3)$$

For the case in which the inhomogeneity effect is so large that $d^2(t+\tau)^2/4 >> 1$, we find from eqs A-1, A-2, and A-3 and from the Condon approximation:

$$\rho_{bv,bv'} = \frac{T_{pu}|\vec{\mu}_{ba}\cdot\vec{E}(\omega_{pu})|^2}{\hbar^2}\sum_u \rho_{au,au}(0)\langle\Theta_{bv}|\Theta_{au}\rangle\langle\Theta_{au}|\Theta_{bv'}\rangle \times \left\{\int_0^\infty d\tau\,\exp\left[-\tau\{i(\bar{\omega}_{bv,au} - \omega_{pu}) + \Gamma^{bv,au}_{bv,au} + \gamma_{pu}\} - \frac{d^2\pi^2}{4}\right] + \int_0^\infty dt\,\exp\left[-\tau\{-i(\bar{\omega}_{bv',au} - \omega_{pu}) + \Gamma^{bv,au}_{bv,au} + \gamma_{pu}\} - \frac{d^2\tau^2}{4}\right]\right\} \quad (A\text{-}4)$$

where $\langle\Theta_{bv}|\Theta_{au}\rangle$ represents the Franck−Condon vibrational overlap integral. Suppose that we are concerned with the vibrational coherence of the ith mode. For this multimode case

$$\langle\Theta_{bv}|\Theta_{au}\rangle = \prod_{l=1}^{N}\langle\chi_{bv_l}|\chi_{au_l}\rangle$$

$$\rho_{bv_i,bv'_i} = \frac{T_{pu}|\vec{\mu}_{ba}\cdot\vec{E}(\omega_{pu})|^2}{\hbar^2}\sum_{u_i}\rho_{au_i,au_i}(0)\langle\chi_{bv_i}|\chi_{au_i}\rangle\langle\chi_{au_i}|\chi_{bv'_i}\rangle \times \left[\int_0^\infty d\tau\,\exp\left[\tau\{i(\omega_{pu} - \bar{\omega}_{bv_i,au_i}) - \Gamma^{bv_i,au_i}_{bv_i,au_i} - \gamma_{pu}\} - \frac{d^2\tau^2}{4}\right]\prod_{l\neq i}G_l(\tau) + \int_0^\infty d\tau\,\exp\left[\tau\{-i(\omega_{pu} - \bar{\omega}_{bv'_i,au_i}) - \Gamma^{bv'_i,au_i}_{bv'_i,au_i} - \gamma_{pu}\} - \frac{d^2\tau^2}{4}\right]\prod_{l\neq i}\{G_l(\tau)\}^*\right] \quad (A\text{-}5)$$

where

$$G_l(t) = \exp[-S_l\{(2\bar{n}_l + 1) - (\bar{n}_l + 1)e^{i\tau\omega_l - \tau\gamma_{1\to 0}} - \bar{n}_l e^{-i\tau\omega_l - \tau\gamma_{1\to 0}}\}] \quad (A\text{-}6)$$

Here $\langle\chi_{bv_i}|\chi_{au_i}\rangle$ represents the Franck−Condon vibrational overlap integral for the $i$the mode, $S_l = (\omega_l/2\hbar)(\Delta Q_l)^2$, $\gamma_{1\to 0} \equiv \gamma_{1_l\to 0_l}(b) \approx \gamma_{1_l\to 0_l}(a)$ (see Appendix B, eq B-9), and $\bar{n}_l = [\exp(\hbar\omega_l/kT) - 1]^{-1}$.

We should stress here that eq A-5 can easily be extended to any number of modes that will be excited coherently. From eq A-5, we can investigate how the rest of the vibrational modes which will not be excited coherently affect the preparation of the vibrational coherence. We can also study effects of inhomogeneity and detuning on the preparation of vibrational coherence by using the dispersion of inhomogeneity distribution which was estimated to be about 150 cm^{-1} for TCNE−HMB complex in CCl_4 solvent in a previous paper.[12]

The band shape functions $F_{bv,bv'}(\omega_{pr})$ and $F_{bv,bv}(\omega_{pr})$ can be derived in a similar fashion;[16,17] for example

$$F_{bv_i,bv'_i}(\omega_{pr}) = \frac{T_2|\vec{\mu}_{ba}\cdot\vec{E}(\omega_{pu})|^2}{\hbar^2}\sum_{u_i}\langle\chi_{au_i}|\chi_{bv_i}\rangle\langle\chi_{bv'_i}|\chi_{au_i}\rangle \times \left[\int_0^\infty d\tau\,\exp\left[\tau\{i(\bar{\omega}_{bv_i,au_i} - \omega_{pr}) - \Gamma^{bv_i,au_i}_{bv_i,au_i} - \gamma_{pr}\} - \frac{d^2\tau^2}{4}\right]\prod_{l\neq i}G_l(\tau) + \int_0^\infty d\tau\,\exp\left[\tau\{-i(\bar{\omega}_{bv'_i,au_i} - \omega_{pr}) - \Gamma^{bv'_i,au_i}_{bv'_i,au_i} - \gamma_{pr}\} - \frac{d^2\tau^2}{4}\right]\prod_{l\neq i}\{G_l(\tau)\}^*\right] \quad (A\text{-}7)$$

Appendix B

This Appendix is mostly concerned with the vibronic coherence created via the electronic coupling between the CT2 and CT1 states. The equation of motion for the vibronic coherence between bv and cw is given by

$$\frac{d}{dt}\rho_{bv,cw}(t) = -\{i(\omega_{bc} + v\omega^b_{vib} - w\omega^c_{vib}) + \Gamma^{v,w}_{v,w}(b,c)\}\rho_{bv,cw}(t) - \Gamma^{v+1,w+1}_{v,w}(b,c)\rho_{bv+1,cw+1}(t) - \Gamma^{v-1,w-1}_{v,w}(b,c)\rho_{bv-1,cw-1}(t) - i\sum_{cw'\neq cw}^{\infty}(J_{bc}/\hbar)\langle bv|cw'\rangle\times\rho_{cw',cw}(t) + i\sum_{bv'\neq bv}^{\infty}(J_{bc}/\hbar)\langle bv'|cw\rangle\rho_{bv,bv'}(t) - i(J_{bc}/\hbar)\langle bv|cw\rangle\{\rho_{cw,cw}(t) - \rho_{bv,bv}(t)\} \quad (B\text{-}1)$$

where vibronic dephasing rate constant $\Gamma^{v,w}_{v,w}(b,c)$ consists of the population decay rate constants $\Gamma^{v,v}_{v,v}(b)$ and $\Gamma^{w,w}_{w,w}(c)$[17,29] and the vibronic pure dephasing rate constant, $\Gamma^{(d)v,w}_{v,w}(b,c)$:

$$\Gamma^{v,w}_{v,w}(b,c) = {}^1/_2\{\Gamma^{v,v}_{v,v}(b) + \Gamma^{w,w}_{w,w}(c)\} + \Gamma^{(d)v,w}_{v,w}(b,c) \quad (B\text{-}2)$$

The vibronic pure dephasing rate constant can be derived by assuming that the system-heat bath interaction is given by $\sum_{\lambda=b,c}|\lambda\rangle Q^2 R^{(2)}(\lambda)\langle\lambda|$, where Q represents the normal coordinate of the system and $R^{(2)}_\lambda$ is a function of the heat bath variables.

In this case, we find

$$\Gamma^{(\mathrm{d})v,w}_{v,w}(b,c) = (v + {}^1\!/_2)^2\gamma^{(d)b} + (w + {}^1\!/_2)^2\gamma^{(d)c} - \left(\frac{v+1/2}{\omega^b_{\mathrm{vib}}}\right)\left(\frac{w+1/2}{\omega^c_{\mathrm{vib}}}\right)\pi\hbar\sum_{\alpha\neq\beta}\sum P_\alpha R^{(2)}_{\alpha\beta}(b)R^{(2)}_{\beta\alpha}(c)\delta(E_{\beta\alpha}) - \left(\frac{v+1/2}{\omega^b_{\mathrm{vib}}}\right)\left(\frac{w+1/2}{\omega^c_{\mathrm{vib}}}\right)\pi\hbar\sum_{\alpha\neq\beta}\sum P_\alpha R^{(2)}_{\alpha\beta}(c)R^{(2)}_{\beta\alpha}(b)\delta(E_{\beta\alpha}) \quad \text{(B-3)}$$

where, for example

$$\gamma^{(d)b} = \frac{\pi\hbar}{(\omega^b_{\mathrm{vib}})^2}\sum_{\alpha\neq\beta}\sum P_\alpha|R^{(2)}_{\alpha\beta}(b)|^2\delta(E_{\beta\alpha}) \quad \text{(B-4)}$$

and $R^{(2)}_{\alpha\beta}(b) = \langle\alpha|R^{(2)}(b)|\beta\rangle$. Here α and β denote the states of the heat bath modes and P_α is the Boltzmann distribution function. $\gamma^{(d)c}$ can be obtained by exchanging b with c in eq B-4.

If we assume that

$$R^{(2)}_{\alpha\beta}(b)R^{(2)}_{\beta\alpha}(c) \approx R^{(2)}_{\alpha\beta}(c)R^{(2)}_{\beta\alpha}(b) \approx |R^{(2)}_{\beta\alpha}(b)|^2 \approx |R^{(2)}_{\beta\alpha}(c)|^2 \equiv |R^{(2)}_{\beta\alpha}|^2 \quad \text{(B-5)}$$

then eq B-3 yields

$$\Gamma^{(\mathrm{d})v,w}_{v,w}(b,c) = \left(\frac{v+{}^1\!/_2}{\omega^b_{\mathrm{vib}}} - \frac{w+{}^1\!/_2}{\omega^c_{\mathrm{vib}}}\right)^2\pi\hbar\sum_{\alpha}\sum_{\beta}P_\alpha R^{(2)}_{\alpha\beta}|^2\delta(E_{\beta\alpha}) \quad \text{(B-6)}$$

Moreover if $\omega^b_{\mathrm{vib}} = \omega^c_{\mathrm{vib}}$ so that $\gamma^{(\mathrm{d})b} = \gamma^{(\mathrm{d})c} \equiv \gamma^{(d)}_{bc}$, we find $\Gamma^{(\mathrm{d})v,w}_{v,w}(b,c) = (v - w)^2\gamma^{(d)}_{bc}$.

In a similar fashion, we can also obtain the rate constant of the vibronic coherence transfer from ($bv + 1$, $cw + 1$) to (bv, cw) as

$$-\Gamma^{v+1,w+1}_{v,w}(b,c) = \frac{\sqrt{(1+v)(1+w)}}{2}\left\{\sqrt{\frac{\omega^c_{\mathrm{vib}}}{\omega^b_{\mathrm{vib}}}}\gamma_{1\to0}(c) + \sqrt{\frac{\omega^b_{\mathrm{vib}}}{\omega^c_{\mathrm{vib}}}}\gamma_{1\to0}(b)\right\} \quad \text{(B-7)}$$

and that from (bv-1, cw-1) to (bv, cw) as

$$-\Gamma^{v-1,w-1}_{v,w}(b,c) = \frac{\sqrt{vw}}{2}\left\{\mathrm{e}^{-\hbar\omega^c_{\mathrm{vib}}/kT}\sqrt{\frac{\omega^c_{\mathrm{vib}}}{\omega^b_{\mathrm{vib}}}}\gamma_{1\to0}(c) + \mathrm{e}^{-\hbar\omega^b_{\mathrm{vib}}/kT}\sqrt{\frac{\omega^b_{\mathrm{vib}}}{\omega^c_{\mathrm{vib}}}}\gamma_{1\to0}(b)\right\} \quad \text{(B-8)}$$

Here $\gamma_{1\to0}(b$ or $c)$ denotes the vibrational relaxation constant and is given by[30]

$$\gamma_{1\to0}(b) = \frac{\pi}{\omega^b_{\mathrm{vib}}}\sum_{\alpha\neq\beta}\sum P_\alpha|R^{(1)}_{\alpha\beta}|^2\delta(E_{\beta\alpha} - \hbar\omega^b_{\mathrm{vib}}) \quad \text{(B-9)}$$

where $\sum_{\lambda=b,c}|\lambda\rangle QR^{(1)}(\lambda)\langle\lambda|$. Here $R^{(1)}(\lambda)$ is a function of heat bath variables.

Appendix C

Here we shall list the important relations between vibrational relaxation and dephasing rate constants:[31]

$$\Gamma^{v,v}_{v,v}(b) = \{v + (1+v)\mathrm{e}^{-\hbar\omega^b_{\mathrm{vib}}/kT}\}\gamma_{1\to0}(b) + \gamma(b) \quad \text{(C-1)}$$

$$-\Gamma^{v+1,v+1}_{v,v}(b) = (v+1)\gamma_{1\to0}(b) \quad \text{(C-2)}$$

$$-\Gamma^{v-1,v-1}_{v,v}(b) = v\mathrm{e}^{-\hbar\omega^b_{\mathrm{vib}}/kT}\gamma_{1\to0}(b) \quad \text{(C-3)}$$

where $\gamma(b)$ represents the radiative decay rate constant. The vibrational dephasing rate constant is given by[31]

$$\Gamma^{v,v'}_{v,v'}(b) = \frac{\Gamma^{v,v}_{v,v}(b) + \Gamma^{v',v'}_{v',v'}(b)}{2} + \Gamma^{(\mathrm{d})v,v'}_{v,v'}(b) \quad \text{(C-4)}$$

with $\Gamma^{(\mathrm{d})v,v'}_{v,v'}(b) = (v - v')^2\gamma^{(d)b}$.

The coherence transfer rate constants are given by[31]

$$-\Gamma^{v+1,v'+1}_{v,v'}(b) = \sqrt{(v+1)(v'+1)}\gamma_{1\to0}(b) \quad \text{(C-5)}$$

$$-\Gamma^{v-1,v-1}_{v,v}(b) = v\mathrm{e}^{-\hbar\omega^b_{\mathrm{vib}}/kT}\gamma_{1\to0}(b) \quad \text{(C-6)}$$

References and Notes

(1) Mulliken R. S.; Person, W. B. *Molecular Complexes*; Wiley: New York, 1969.
(2) Briegleb, G. *Elektronen-Donator-Accpetor-Komplexe*; Springer-Verlag: Berlin, 1961; p 50.
(3) Voigt, E. M. *J. Am. Chem. Soc*, **1964**, *86*, 3611.
(4) Mataga N.; Kubota, T. *Molecular Interactions and Electronic Spectra*; Marcel Dekker: New York, 1970.
(5) Markel, F.; Ferris, N. S.; Gould, I. R.; Myers, A. B. *J. Am. Chem. Soc*. **1992**, *114*, 6208.
(6) Kulinowski, K.; Gould, I. R.; Myers, A. B. *J. Phys. Chem.* **1995**, *99*, 9017.
(7) Kulinowski, K.; Gould I. R.; Ferris N. S.; Myers A. B. *J. Phys. Chem*. **1995**, *99*, 17715.
(8) Britt, B. M.; Lueck, H. B.; McHale, J. L. *Chem. Phys. Lett*. **1992**, *190*, 528.
(9) Smith, M. L.; Mchale, J. L. *J. Phys. Chem.* **1985**, *89*, 4002.
(10) Mchale, J. L.; Merriam, M. J. *J. Phys. Chem.* **1989**, *93*, 526.
(11) Britt, B. M.; McHale, J. L.; Friedrich D. M. *J. Phys. Chem.* **1995**, *99*, 6347.
(12) Hayashi, M.; Yang, T.-S.; Yu, J.; Mebel, A; Lin, S. H. *J. Phys. Chem.* **1997**, *101*, 4156.
(13) Wynne, K.; Galli, C.; Hochstrasser R. M. *J. Chem. Phys*. **1994**, *100*, 4797.
(14) Rubtsov, I. V.; Yoshihara, K. *J. Phys. Chem.* **1997**, *101*, 6138.
(15) Fan, B.; Lin, S. H.; Hamer, N. *J. Chem. Phys.* **1989**, *91*, 4485.
(16) Lin, S. H.; Fan, B.; Hamer, N. *Adv. Chem. Phys.* **1990**, *79*, 133.
(17) Lin, S. H.; Alden, A.; Islampour R.; Ma H.; Villaeys, A. A. *Density Matrix Method and Femtosecond Processes*; World Scientific: Singapore, 1991.
(18) Suzuki, S.; Sung, H. C.; Hayashi, M.; Lin, S. H. *Physica A* **1995**, *221*, 15.
(19) Sugawara, M.; Fujimura. Y.; Yen, C. Y.; Lin. S. H. *J. Photochem. Photobiol*. **1990**, *A54*, 321.
(20) Gu, X. Z.; Hayashi, M.; Suzuki, S.; Lin, S. H. *Biochim. Biophys. Acta* **1995**, *1229*, 215.
(21) Sugawara, M.; Hayashi, M.; Suzuki, S.; Lin, S. H. *Mol. Phys.* **1996**, *87*, 637.
(22) Lin, S. H.; Fain, B.; Yeh, C. Y. *Phys. Rev.* **1990**, *41A*, 2718.
(23) Mitsunaga, M.; and Tang, C. L. *Phys. Rev.* **1987**, *35A*, 1720.
(24) Walmsley, I. A.; Mitsunaga, M.; Tang, C. J. *Phys. Rev.* **1988**, *38A*, 4681.
(25) Walmsley, L. A.; Wise F. W.; Tang, C. L. *Chem. Phys. Lett.* **1989**, *154*, 315.

(26) Kim, Y. R.; Share, P.; Pereira, M.; Sarisky, M.; Hochstrasser, R. M. *J. Chem. Phys.* **1989**, *91*, 7557.
(27) Zhu, F.; Galli, C.; Hochstrasser, R. M.; *J. Chem. Phys.* **1993**, *98*, 1042.
(28) Wynne K.; Hochstrasser, R. M. *Chem. Phys.* **1993**, *171*, 179.
(29) Fujimura, Y. In *Advances in Multi-photon Processes and Spectroscopy*; Lin, S. H., Ed.; World Scientific: Singapore, 1986; Vol. 2, p 1.
(30) Lin, S. H. *J. Chem. Phys.* **1974**, *61*, 3810.
(31) Hayashi, M.; Yang, T.-S.; Mebel, A.; Chang, C. H.; Lin, S. H.; Scherer, N. F. *Chem. Phys.* **1997,** *217*, 259.